Advances in Applied Mathematics and Mechanics
Adv. Appl. Math. Mech., Vol. **16**, No. 2, pp. 549-568

DOI: 10.4208/aamm.OA-2022-0056
April 2024

Effect of Thermal Convection and Mass Transfer on Particle Motion during Sedimentation: A Numerical Study

Junjie Hu[1,2,*] and Dongke Sun[1]

[1] *School of Mechanical Engineering, Southeast University, Nanjing, Jiangsu 211189, China*
[2] *Hubei Key Laboratory of Engineering Modeling and Scientific Computing, Huazhong University of Science and Technology, Wuhan, Hubei 430074, China*

Received 2 March 2022; Accepted (in revised version) 26 March 2023

Abstract. The sedimentation of a particle cluster with heat and mass transfer is studied with the lattice Boltzmann method. To investigate the effect of thermal convection and mass transfer on the motion of the particle cluster, four cases are studied, namely, without heat and mass transfer, with heat transfer, with mass transfer and with heat and mass transfer. Compared to mass transfer, the effect of thermal convection is more dominant, which affects the motion of the particle cluster significantly. The particle-particle interaction is enforced by thermal convection, and the oscillation of the average settling velocity of the particle cluster is more intense. Besides, with mass transfer between the particles and the fluid, the mass of the particles decreases, the motion of the particles is more sensitive to the fluid flow, the velocity fluctuation of the particle cluster is more intense, the distribution of the particle cluster is more inhomogeneous.

AMS subject classifications: 35Q30, 76D05

Key words: Particle sedimentation, thermal convection, mass transfer, lattice Boltzmann method.

1 Introduction

The motion of inertial particles in the fluid is ubiquitous, which plays a key role in industrial and natural sciences, and thus the sediment dynamics is studied by numerous researchers [1–4]. For example, Feng et al. [1] studied the sedimentation of numerous circular particles, and reported the Rayleigh-Taylor instability during the sedimentation. Zaidi et al. [2] investigated the average settling velocity of the particle cluster, and pointed out that the inhomogeneous particle distribution affected the average settling velocity of

*Corresponding author.
Email: hujunjie@cug.edu.cn (J. Hu)

the particle cluster significantly. Zhang et al. [3] studied the sedimentation of a particle pair in a shear-thinning power-law fluid with the multiple-relaxation-time lattice Boltzmann method, and reported that the particle pair experienced several different movement states depending on the initial geometrical configuration. To deepen the understanding of the entrainment mechanism, Li et al. [4] conducted a two-dimensional numerical investigation of the particle entrainment in the presence of a large downstream circular obstacle. However, under some cases, like coal combustion and food processing, the particle and the fluid are non-isothermal, meanwhile, the particle is composed of different components, some insoluble while some soluble in the fluid, besides the hydrodynamic force, the particle motion is affected by thermal convection and mass transfer.

Some researchers investigated the effect of thermal convection on the particle motion [5–14]. For example, Gan et al. [5] studied a cold particle settling in a vertical channel with the finite element method, and reported that the settling behavior of the particle is significantly different from the isothermal case. Gan et al. pointed out that the settling behavior of the non-isothermal particle was the competitive result between forced convection and thermal convection. Mandujano et al. [7] studied thermal levitation, namely, a particle with a density slightly different from the fluid kept still at the steady state due to thermal convection, and discussed the stability of thermal levitation. Wang et al. [9] studied convective heat transfer between gas and a particle cluster in a circulating fluidized bed riser, and pointed out that the heat flux of the individual particle inside the cluster was smaller than that of an isolated particle. At the same time, they reported that the convective heat transfer coefficient increased with the increase of the porosity of the particle cluster, because more gas passed through the particle cluster.

Though some researchers studied mass transfer between the particle and the fluid, the focus is limited to the rate of mass transfer [15–19], while the effect of mass transfer on the particle motion is investigated rarely. For example, Wang et al. [18] studied mass transfer between air and a particle cluster in a circulating fluidized bed, and pointed out that the rate of mass transfer was reduced due to the particle clustering, since less air passed through the particle cluster. In the study, the particle cluster is fixed and the uniform air flow is imposed at the inlet, thus, the particle motion and mass transfer is decoupled artificially. However, the reality is that the particle properties, such as density, mass and moment inertia, will vary with mass transfer between the particle and the fluid, which affects the particle motion significantly.

During the sedimentation of the particles with heat and mass transfer, like coal combustion and food processing, the temperature and concentration distribution is related to the fluid flow, which affects the particle motion, conversely, the particle motion affects the fluid flow, temperature and concentration distribution. Thus, the sedimentation of the particle cluster with heat and mass transfer is complex, where the fluid flow, particle motion, thermal convection and mass transfer affect each other.

The rest of the paper is organized as follows. Section 2 describes the problem, Section 3 introduces the numerical method, and Section 4 validates our code. Section 5 are the results and discussions, where the effect of thermal convection and mass transfer on the

particle motion is investigated, and Section 6 gives some conclusions.

2 Problem description

Fig. 1 is the diagram of the sedimentation of a particle cluster with heat and mass transfer. The size of the channel is $W\times H=5\text{cm}\times 50\text{cm}$. The particle cluster is composed of N identical particles, which are randomly distributed in a circular domain with diameter $D_c=10D_p$, where $D_p=0.25\text{cm}$ is the diameter of the particle.

To generate the random particle cluster, the Hard-Sphere Monte-Carlo (HSMC) method [20, 21] is adopted. In the HSMC method, the initial positions of the particles inside the circular domain obey the random distribution, and the overlapping between the particles is forbidden. Firstly, we generate a pair of random numbers to designate the initial positions of the particles, then, we need to determine whether there is overlapping between the particles. If there is no overlapping, we add the particle to the circular domain, otherwise, we delete it and generate a new one, until the particle number is satisfied. Fig. 2 shows the random particle cluster generated with the HSMC method, where the particle number $N=15$.

The particle and the fluid are non-isothermal, and there is thermal convection between them. To observe the long-time effect of thermal convection, the temperature of the particles is $T_s=0$, while the temperature of the channel walls and the initial temperature of the fluid are $T_w=1$. Besides, to make the problem simple, the particle is composed of two components, one insoluble while the other soluble, and there is mass transfer between the particle and the fluid. The insoluble component is undeformable, which forms the particle shell. The rate of mass transfer across the particle surface is [15]

$$\frac{dm_s}{dt}=-\oint_\Gamma D\nabla C\cdot\boldsymbol{n}ds, \tag{2.1}$$

where m_s is the mass of the soluble component in the particle, D is the mass diffusivity, ∇C is the concentration gradient of the soluble component, and $\boldsymbol{n}$ is the unit vector

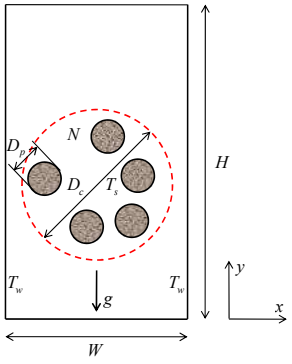

Figure 1: Sedimentation of a particle cluster with heat and mass transfer.

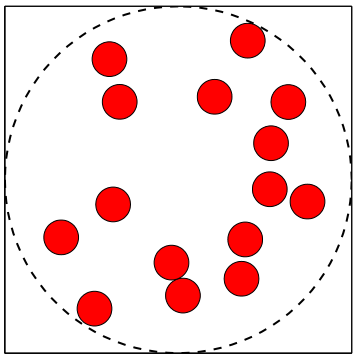

Figure 2: Initial distribution of the random particle cluster, where the particle number $N=15$.

normal to the particle surface. With mass transfer between the particle and the fluid, the mass of the soluble component in the particle decreases, leading to a decreasing concentration of the soluble component at the particle surface, which is determined by the mass ratio of the soluble component γ, namely,

$$C_s=\gamma=\frac{m_s(t)}{m_s(0)}, \tag{2.2}$$

where $m_s(0)$ is the initial mass of the soluble component in the particle. With mass transfer between the particle and the fluid, the particle mass varies. Initially, the particle mass is composed of two parts,

$$m_p(0)=m_i+m_s(0), \tag{2.3}$$

where m_i is the mass of the insoluble component in the particle, which is a constant. With the soluble component diffusing in the fluid, the dissolved volume is occupied by the fluid, and the particle mass includes three parts,

$$m_p(t)=m_i+m_s(t)+m_f(t), \tag{2.4}$$

where $m_f(t)$ is the mass of the fluid to occupy the dissolved volume. Assuming that both the fluid and the soluble component are incompressible, the mass of the fluid is

$$m_f(t)=\rho_f\frac{m_s(0)-m_s(t)}{\rho_s}, \tag{2.5}$$

where $\rho_f=1.0\text{g/cm}^3$ is the density of the fluid, and ρ_s is the density of the soluble component. Since the insoluble component is undeformable, the particle shape and size are kept unchanged, thus, the density and moment inertia of the particle vary. The particle is composed of two components, including the density of the insoluble component $\rho_i=1.05\text{g/cm}^3$ and the density of the soluble component $\rho_s=1.05\text{g/cm}^3$, and the density

of the composite particle is the volume average of these two components. The soluble component distributes uniformly inside the particle, and its initial volume fraction is $\epsilon_0 = 0.1$.

The relevant dimensionless numbers are

- Prandtl number
$$\mathrm{Pr} = \frac{\nu}{\alpha} = 0.7. \tag{2.6}$$

- Grashof number
$$\mathrm{Gr} = \frac{g\beta D_p^3 (T_w - T_s)}{\nu^2} = 1000. \tag{2.7}$$

- Schmidt number
$$\mathrm{Sc} = \frac{\nu}{D} = 10, \tag{2.8}$$

where $\nu = 0.1\mathrm{cm}^2/\mathrm{s}$ is the kinematic viscosity of the fluid, α is the thermal diffusivity of the fluid, g=980cm/s^2 is the gravity acceleration, β is the thermal expansion coefficient of the fluid, and D is the mass diffusivity. The Grashof number reflects the strength of thermal convection, with Gr increasing, thermal convection becomes stronger. The Schmidt number describes the rate of mass transfer, with Sc increasing, the mass diffusivity decreases, thus, mass transfer becomes slower.

3 Numerical method

3.1 Lattice Boltzmann method for flows with heat and mass transfer

To couple the fluid flow, heat and mass transfer, the multi-distribution-function lattice Boltzmann method is adopted, and the evolution equations are

$$f_i(\boldsymbol{x}+\boldsymbol{c}_i\delta t, t+\delta t) - f_i(\boldsymbol{x},t) = -\frac{1}{\tau_f}(f_i - f_i^{eq}) + \delta t F_i, \tag{3.1a}$$

$$g_i(\boldsymbol{x}+\boldsymbol{c}_i\delta t, t+\delta t) - g_i(\boldsymbol{x},t) = -\frac{1}{\tau_g}(g_i - g_i^{eq}), \tag{3.1b}$$

$$h_i(\boldsymbol{x}+\boldsymbol{c}_i\delta t, t+\delta t) - h_i(\boldsymbol{x},t) = -\frac{1}{\tau_h}(h_i - h_i^{eq}), \tag{3.1c}$$

where $f_i(\boldsymbol{x},t)$, $g_i(\boldsymbol{x},t)$ and $h_i(\boldsymbol{x},t)$ are the distribution functions of the fluid flow, temperature and concentration fields, respectively, f_i^{eq}, g_i^{eq} and h_i^{eq} are the equilibrium distribution functions, τ_f, τ_g and τ_h are the dimensionless relaxation times, δt is the time step, and F_i is the added body force related to the temperature difference. Adopting the D2Q9

(2-dimension and 9-velocity) model [22], the equilibrium distribution functions are

$$f_i^{eq}(\rho,\boldsymbol{u})=w_i\rho\left[1+\frac{\boldsymbol{c}_i\cdot\boldsymbol{u}}{c_s^2}+\frac{(\boldsymbol{c}_i\cdot\boldsymbol{u})^2}{2c_s^4}-\frac{\boldsymbol{u}\cdot\boldsymbol{u}}{2c_s^2}\right], \tag{3.2a}$$

$$g_i^{eq}(T,\boldsymbol{u})=w_iT\left[1+\frac{\boldsymbol{c}_i\cdot\boldsymbol{u}}{c_s^2}+\frac{(\boldsymbol{c}_i\cdot\boldsymbol{u})^2}{2c_s^4}-\frac{\boldsymbol{u}\cdot\boldsymbol{u}}{2c_s^2}\right], \tag{3.2b}$$

$$h_i^{eq}(C,\boldsymbol{u})=w_iC\left[1+\frac{\boldsymbol{c}_i\cdot\boldsymbol{u}}{c_s^2}+\frac{(\boldsymbol{c}_i\cdot\boldsymbol{u})^2}{2c_s^4}-\frac{\boldsymbol{u}\cdot\boldsymbol{u}}{2c_s^2}\right], \tag{3.2c}$$

where

$$w_i=\begin{cases}4/9, & i=0,\\ 1/9, & i=1,2,3,4,\\ 1/36, & i=5,6,7,8,\end{cases} \tag{3.3}$$

is the weight parameter of the model,

$$\boldsymbol{c}_i=\begin{cases}(0,0), & i=0,\\ c(\cos[(i-1)\pi/2],\sin[(i-1)\pi/2]), & i=1,2,3,4,\\ \sqrt{2}c(\cos[(2i-1)\pi/4],\sin[(2i-1)\pi/4]), & i=5,6,7,8,\end{cases} \tag{3.4}$$

is the discrete velocity of the model, $c_s=c/\sqrt{3}$ is the sound speed, $c=\delta x/\delta t$, and δx is the space step.

To reflect the effect of thermal convection, the Boussinesq approximation is adopted, where the fluid density depends on the temperature linearly, namely,

$$\rho=\rho_0[1-\beta(T-T_w)]. \tag{3.5}$$

The fluid gravity of unit volume is

$$\boldsymbol{G}=\rho\boldsymbol{g}=\rho_0[1-\beta(T-T_w)]\boldsymbol{g}=\rho_0\boldsymbol{g}-\rho_0\boldsymbol{g}\beta(T-T_w), \tag{3.6}$$

where $\rho_0\boldsymbol{g}$ is the fluid gravity at the temperature T_w, and

$$\boldsymbol{F}=-\rho_0\boldsymbol{g}\beta(T-T_w) \tag{3.7}$$

is the added body force related to the temperature difference, which is discretized with Guo's scheme [23], namely,

$$F_i=w_i\left(\frac{\boldsymbol{c}_i-\boldsymbol{u}}{c_s^2}+\frac{\boldsymbol{c}_i\cdot\boldsymbol{u}}{c_s^4}\boldsymbol{c}_i\right)\cdot\boldsymbol{F}. \tag{3.8}$$

To acquire the density, velocity, temperature of the fluid and concentration of the soluble component, we calculate the moment of the distribution functions, namely,

$$\rho=\sum_i f_i, \qquad \boldsymbol{u}=\frac{1}{\rho}\left(\sum_i\boldsymbol{c}_if_i+\frac{\delta t}{2}\boldsymbol{F}\right), \tag{3.9a}$$

$$T=\sum_i g_i, \qquad C=\sum_i h_i. \tag{3.9b}$$

With the multi-scale analysis [24], the macroscopic governing equations are acquired, namely,

$$\frac{\partial \rho}{\partial t}+\nabla\cdot(\rho \boldsymbol{u})=0, \tag{3.10a}$$

$$\frac{\partial \boldsymbol{u}}{\partial t}+(\boldsymbol{u}\cdot\nabla)\boldsymbol{u}=-\frac{1}{\rho}\nabla p+\nu\nabla^2\boldsymbol{u}+\boldsymbol{F}, \tag{3.10b}$$

$$\frac{\partial T}{\partial t}+\nabla\cdot(T\boldsymbol{u})=\nabla\cdot(\alpha\nabla T), \tag{3.10c}$$

$$\frac{\partial C}{\partial t}+\nabla\cdot(C\boldsymbol{u})=\nabla\cdot(D\nabla C), \tag{3.10d}$$

where the first two equations are the Navier-Stokes equations, which describe the fluid flow, and the third and forth equations are the convection-diffusion equations of the temperature and concentration fields. The macroscopic transport coefficients are related to the dimensionless relaxation times, namely,

$$\nu=c_s^2\left(\tau_f-\frac{1}{2}\right)\delta t, \tag{3.11a}$$

$$\alpha=c_s^2\left(\tau_g-\frac{1}{2}\right)\delta t, \tag{3.11b}$$

$$D=c_s^2\left(\tau_h-\frac{1}{2}\right)\delta t. \tag{3.11c}$$

3.2 Unified iterative scheme for moving boundaries

For the sedimentation of the particle cluster, the treatment of moving boundaries is crucial [25,26]. In the lattice Boltzmann method, the moving boundary treatment is classified into two categories, including diffuse boundary treatment [1,27,28] and sharp boundary treatment. In the diffuse boundary treatment, the thickness of the boundary is nonzero, and the numerical boundary is not always the physical boundary, comparatively, the sharp boundary treatment is of better numerical accuracy. In the present study, the sharp boundary treatment is adopted, where the Euler grid is fixed, and two types of nodes need to be specified, including boundary nodes around the particle and fresh fluid nodes due to the movement of the particle. Fig. 3 depicts these two types of nodes. To treat these two types of nodes consistently, the unified iterative scheme for moving boundaries [29] is adopted.

After a time step, the distribution functions at fluid nodes and boundary nodes with links to other fluid nodes are updated. At a boundary node or a fresh fluid node, the unknown distribution functions are constructed with two steps, namely, prediction step and correction steps. In the prediction step, the unknown distribution functions are approximated with those at their neighboring nodes, namely, $f_i(\boldsymbol{x}_f)=f_i(\boldsymbol{x}_{ff})$. To reflect the boundary effect, the correction step is conducted, where the distribution functions

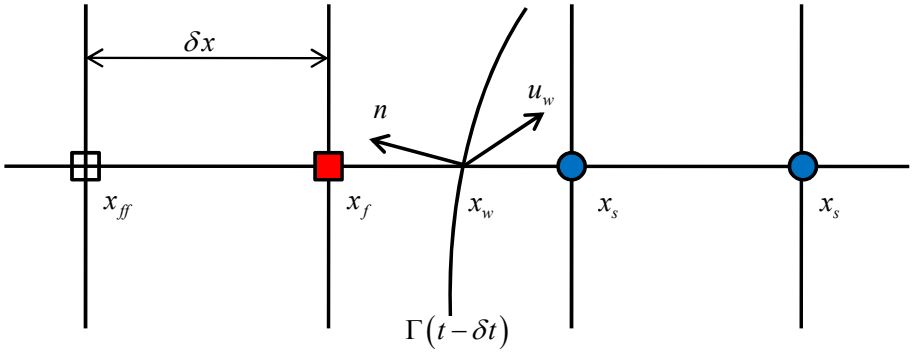

(a) The filled square is the boundary node $\boldsymbol{x}_f$, the hollow square is the fluid node $\boldsymbol{x}_{ff}$, and the filled circle is the solid node $\boldsymbol{x}_s$ inside the particle

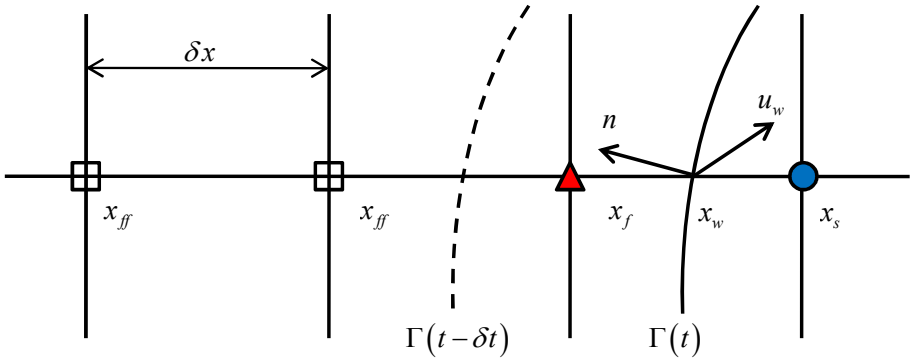

(b) Due to the movement of the particle, the solid node $\boldsymbol{x}_s$ at $t-\delta t$ becomes a fresh fluid node $\boldsymbol{x}_f$ at t

Figure 3: Boundary nodes around the particle (a) and fresh fluid nodes due to the movement of the particle (b).

are decomposed into their equilibrium parts and non-equilibrium parts. After the prediction step, the unknown distribution functions at node $\boldsymbol{x}_f$ are approximated, thus, the fluid density and velocity at node $\boldsymbol{x}_f$ are known, including the equilibrium parts $f_i^{eq}(\boldsymbol{x}_f)$ and non-equilibrium parts $f_i^{ne}(\boldsymbol{x}_f)$. The fluid density at point $\boldsymbol{x}_w$ is approximated with that at node $\boldsymbol{x}_f$, namely, $\rho_w \approx \rho_f$, and the fluid velocity at point $\boldsymbol{x}_w$ is calculated with $\boldsymbol{u}_w = \boldsymbol{u}_p + \boldsymbol{\omega}_p \times (\boldsymbol{x}_w - \boldsymbol{x}_p)$, where $\boldsymbol{u}_p$ and $\boldsymbol{\omega}_p$ are the translational and rotational velocities of the solid particle, respectively, and $\boldsymbol{x}_p$ is the position of the solid particle. With the fluid density and velocity at point $\boldsymbol{x}_w$ known, the equilibrium parts $f_i^{eq}(\boldsymbol{x}_w)$ are acquired, and the non-equilibrium parts are approximated with those at node $\boldsymbol{x}_f$, that is, $f_i^{ne}(\boldsymbol{x}_w) = f_i^{ne}(\boldsymbol{x}_f)$. Then, the fictitious distribution functions at point $\boldsymbol{x}_w$ are constructed, namely, $f_i(\boldsymbol{x}_w) = f_i^{eq}(\boldsymbol{x}_w) + f_i^{ne}(\boldsymbol{x}_w)$. To correct the unknown distribution functions at node

$\boldsymbol{x}_f$, a first-order interpolation is adopted, namely,

$$f_i(\boldsymbol{x}_f) = [qf_i(\boldsymbol{x}_{ff}) + f_i(\boldsymbol{x}_w)]/(q+1), \tag{3.12}$$

where $q = |\boldsymbol{x}_f - \boldsymbol{x}_w|/|\boldsymbol{x}_f - \boldsymbol{x}_s|$ is the fraction of the intersected link in the fluid region. To improve the numerical accuracy and decrease the inconsistency between the constructed distribution functions and those evolutionary ones, the enforced iteration is adopted. In each iteration step, the correction step is executed, and the unknown distribution functions at node $\boldsymbol{x}_f$ are updated.

Though the unified iterative scheme for moving boundaries is designed for flows without heat and mass transfer, extending it to the temperature and concentration boundaries is straightforward [30]. Similarly, to construct the unknown distribution functions at node $\boldsymbol{x}_f$, the prediction step and correction step are conducted. In the prediction step, we approximate the unknown distribution functions at node $\boldsymbol{x}_f$ with those at their neighboring nodes. In the correction step, instead of the fluid density, we use the temperature and concentration at point $\boldsymbol{x}_w$ to construct the equilibrium distribution functions. After the unknown distribution functions are constructed, the enforced iteration is adopted.

3.3 Hydrodynamic force on a solid particle

To update the velocity and position of the particle accurately, evaluating the hydrodynamic force on a solid particle is crucial. Here, the Galilean invariant momentum exchange method is adopted [31]. As depicted in Fig. 4, the momentum carried by the fluid particle toward the solid surface before the collision is $(\boldsymbol{c}_i - \boldsymbol{u}_w) f_i^+(\boldsymbol{x}_f, t)$ relative to the solid surface, while the relative momentum is $(\boldsymbol{c}_{-i} - \boldsymbol{u}_w) f_{-i}(\boldsymbol{x}_f, t+\delta t)$ after the collision with the solid surface, where $f_i^+(\boldsymbol{x}_f, t)$ is the post-collision distribution function at time t, and $f_{-i}(\boldsymbol{x}_f, t+\delta t)$ is the updated distribution function at time $t+\delta t$. Thus, the hydrodynamic force on the solid particle is

$$\boldsymbol{F} = \sum_{\boldsymbol{x}_f} \sum_i [(\boldsymbol{c}_i - \boldsymbol{u}_w) f_i^+(\boldsymbol{x}_f, t) - (\boldsymbol{c}_{-i} - \boldsymbol{u}_w) f_{-i}(\boldsymbol{x}_f, t+\delta t)], \tag{3.13}$$

and the torque is

$$T = \sum_{\boldsymbol{x}_f} \sum_i \{(\boldsymbol{x}_w - \boldsymbol{x}_p) \times [(\boldsymbol{c}_i - \boldsymbol{u}_w) f_i^+(\boldsymbol{x}_f, t) - (\boldsymbol{c}_{-i} - \boldsymbol{u}_w) f_{-i}(\boldsymbol{x}_f, t+\delta t)]. \tag{3.14}$$

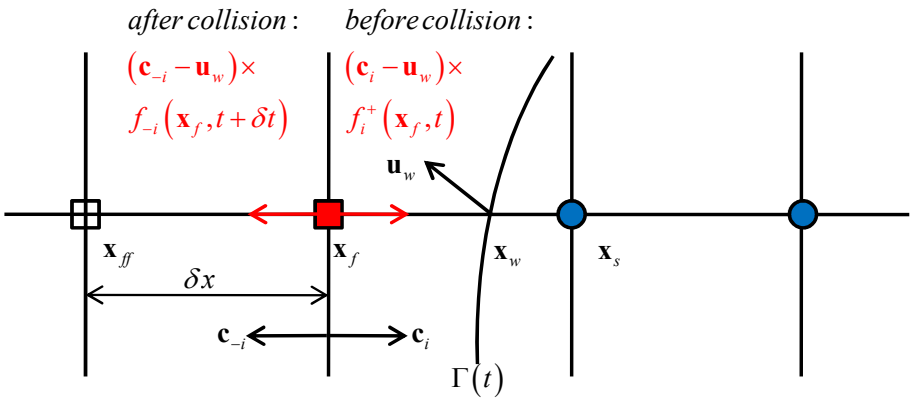

Figure 4: Sketch of the Galilean invariant momentum exchange method.

3.4 Particle-particle and particle-wall interaction

During the sedimentation of the particle cluster, to avoid the particle-particle overlapping, the particle-particle interaction is treated with the collision model [32],

$$\boldsymbol{F}_{i,j}^p = \begin{cases} 0, & d_{i,j} > D_p + \zeta, \\ \dfrac{1}{\epsilon_p}(\boldsymbol{x}_i - \boldsymbol{x}_j)(D_p + \zeta - d_{i,j})^2, & D_p \le d_{i,j} \le D_p + \zeta, \\ \dfrac{1}{\epsilon_p'}(\boldsymbol{x}_i - \boldsymbol{x}_j)(D_p - d_{i,j}), & d_{i,j} < D_p, \end{cases} \tag{3.15}$$

where $d_{i,j} = |\boldsymbol{x}_i - \boldsymbol{x}_j|$ is the distance between the particles, ζ is the threshold of the particle-particle interaction, which is set to be δx, $\epsilon_p = (\delta x)^2$ and $\epsilon_p' = \delta x$ are the stiff parameters. Similarly, to avoid the particle-wall overlapping, the collision model of the particle-wall interaction is

$$\boldsymbol{F}_i^w = \begin{cases} 0, & d_i' > D_p + \zeta, \\ \dfrac{1}{\epsilon_w}(\boldsymbol{x}_i - \boldsymbol{x}_i')(D_p + \zeta - d_i')^2, & D_p \le d_i' \le D_p + \zeta, \\ \dfrac{1}{\epsilon_w'}(\boldsymbol{x}_i - \boldsymbol{x}_i')(D_p - d_i'), & d_i' < D_p, \end{cases} \tag{3.16}$$

where $\boldsymbol{x}_i'$ is the image position of the particle about the wall, $d_i' = |\boldsymbol{x}_i - \boldsymbol{x}_i'|$ is the distance between the particle and its image, $\epsilon_w = \epsilon_p/2$ and $\epsilon_w' = \epsilon_p'/2$ are the stiff parameters of the particle-wall interaction.

3.5 Particle motion equations

To update the velocity and position of the particle, the particle motion equations are

$$m_i\frac{d\boldsymbol{u}_i}{dt}=m\boldsymbol{g}+\boldsymbol{F}_i^b+\boldsymbol{F}_i^h+\sum_{j=1,j\neq i}^{N}\boldsymbol{F}_{i,j}^p+\boldsymbol{F}_i^w, \tag{3.17a}$$

$$I_i\frac{d\omega_i}{dt}=T_i^h,\quad \frac{d\boldsymbol{x}_i}{dt}=\boldsymbol{u}_i,\quad \frac{d\theta_i}{dt}=\omega_i, \tag{3.17b}$$

where $\boldsymbol{u}_i$ and ω_i are the translational and rotational velocities of the i-th particle, respectively, $\boldsymbol{x}_i$ and θ_i are the translational and rotational positions, respectively, m_i and I_i are the mass and moment inertia, respectively, $\boldsymbol{F}_i^b$ is the buoyancy force, $\boldsymbol{F}_i^h$ is the hydrodynamic force, $\sum_{j=1,j\neq i}^{N}\boldsymbol{F}_{i,j}^p$ and $\boldsymbol{F}_i^w$ are from the particle-particle and particle-wall interaction, respectively.

4 Code validation

To validate our code, two problems are selected, namely, a cold particle settling in a vertical channel and a particle with concentration convection-diffusion moving in a horizontal channel.

4.1 A cold particle settling in a vertical chanel

The problem was firstly investigated by Gan et al. [5] with the finite-element method, after that, many researchers validated their numerical methods with the problem [10–14]. A particle with diameter $D_p=25\delta x$ is located in a vertical channel with width $W=4D_p$ and height $H=320D_p$. Initially, the particle is positioned off the centerline of the channel by half the diameter. The density ratio of the particle to the fluid is $\rho_r=\rho_p/\rho_f=1.00232$. The reference Reynolds number $\mathrm{Re}_r=D_pU_r/\nu$ is set to be 40.5, where $U_r=\sqrt{\pi(D_p/2)(\rho_r-1)g}$ is the reference velocity. The temperature of the particle is kept at $T_s=0$, and the temperature of the channel walls is kept at $T_w=1$. Fig. 5 shows the time history of the lateral position of the particle at different Gr. At $810<\mathrm{Gr}<2150$, the centerline of the channel is not the equilibrium position of the particle, instead, a steady settling of the particle closer to the side wall is observed, which is in agreement with Gan's report [5] qualitatively.

4.2 A particle with concentration convection-diffusion moving in a horizontal channel

Furthermore, a particle with concentration convection-diffusion moving in a horizontal channel is simulated [33]. A particle with diameter $D_p=80\delta x$ moves in a horizontal channel with width $W=2D_p$ along the centerline with a constant velocity $U_0=5\times10^{-3}$.

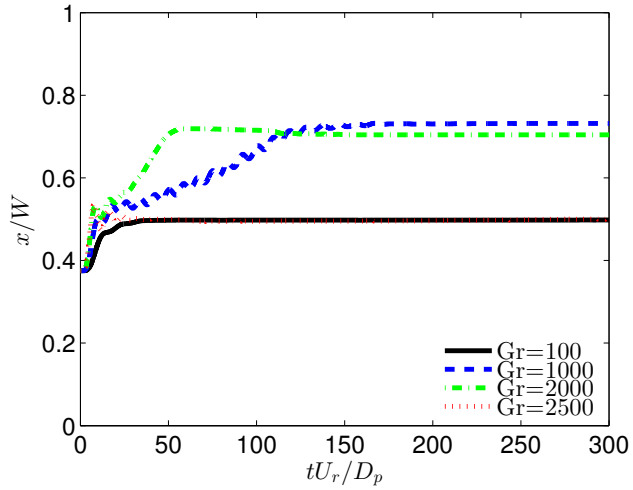

Figure 5: Time history of the lateral position of the particle at different Gr.

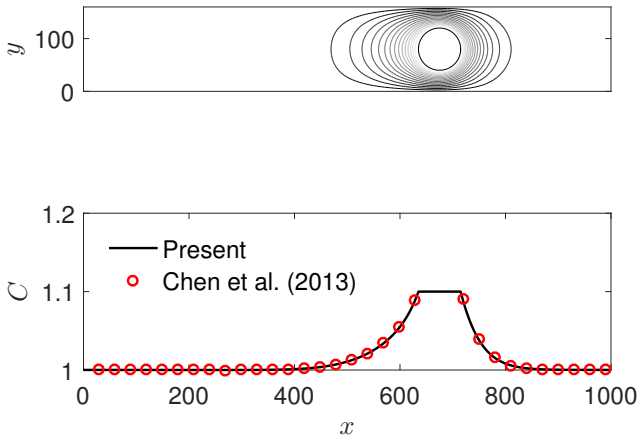

Figure 6: Concentration distribution around the particle surface (top) and concentration profile along the centerline (bottom).

The concentration at the particle surface is fixed at $C_s = 1.1$, while the concentration at the channel walls is kept at $C_w = 1.0$. At the inlet and outlet of the channel, the periodic boundary condition is adopted. Fig. 6 shows the concentration distribution around the particle surface and the concentration profile along the centerline. The concentration distribution about the particle is asymmetric, which is from the effect of the convection on the diffusion process. It is observed that the agreement of the concentration profile along the centerline between our result and the literature data [33] is great.

5 Results and discussions

To investigate the effect of thermal convection and mass transfer on the motion of the particle cluster, four cases are studied, namely, without heat and mass transfer, where the motion of the particle cluster is affected by the fluid flow, with heat transfer, where the motion of the particle cluster is affected by the fluid flow and thermal convection, with mass transfer, where the motion of the particle cluster is affected by the fluid flow and mass transfer, and with heat and mass transfer, where the motion of the particle cluster is affected by the fluid flow, thermal convection and mass transfer.

Firstly, to describe the motion of the particle cluster quantitatively, the average settling velocity of the particle cluster is calculated,

$$\overline{\boldsymbol{u}}=(\overline{u},\overline{v})=\frac{1}{N}\sum_i \boldsymbol{u}_i. \tag{5.1}$$

Fig. 7 shows the time history of the average settling velocity of the particle cluster in the horizontal and vertical directions. In the horizontal direction, it is observed that $\overline{u}$ oscillates around zero. At the beginning, the particles distribute closely, the particle-particle interaction is strong, which is apt to disperse the particles. However, with the particles moving toward the channel walls, the confinement of the channel walls becomes significant, which suppresses the dispersion of the particles, consequently, the particles are forced to move toward the channel centerline, and $\overline{u}$ oscillates around zero. Furthermore, compared to the cases without heat transfer, the oscillation of $\overline{u}$ of the cases with heat transfer is much more intense. In the vertical direction, $\overline{v}$ experiences two phases, namely, monotonic increase and oscillation. At the beginning, the particle cluster moves like a single particle, and $\overline{v}$ increases monotonically.

With the settling velocity of the particles increasing, the drag force increases rapidly, which decelerates the particles, after a transient overshoot, the particle-particle interaction becomes stronger, and the particles move disorderly, which leads to the oscillation of $\overline{v}$. Compared to the cases without heat transfer, it is observed that $\overline{v}$ of the cases with heat transfer oscillates much more intensely, which is attributed to thermal convection between the particles and the fluid.

Fig. 8 shows the vortex distribution around the particles at $t/(D_p^2/\nu)=2$. It is observed that the vortex distribution around the particles of the cases with heat transfer is quite different from that of the cases without heat transfer. Compared to the cases without heat transfer, under the effect of thermal convection, the particles distribute much loosely. Furthermore, Fig. 9 shows the temperature distribution around the particles at $t/(D_p^2/\nu)=2$. The temperature of the particles is lower than that of the fluid, and the fluid around the particles is cooled. With the fluid temperature decreasing, the fluid density increases, which leads to an added body force, namely, thermal buoyancy force. Under the effect of thermal buoyancy force, a downward fluid flow occurs, namely, thermal convection, which pushes the particles to move downward, consequently, $\overline{v}$ of the cases with heat transfer is larger than that of the cases without heat transfer. Meanwhile, with the

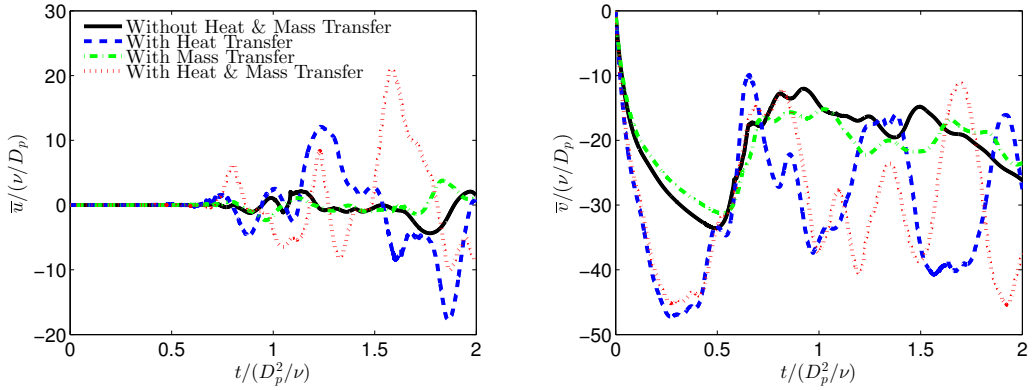

(a) Horizontal direction (b) Vertical direction

Figure 7: Time history of the average settling velocity of the particle cluster in the horizontal (a) and vertical (b) directions.

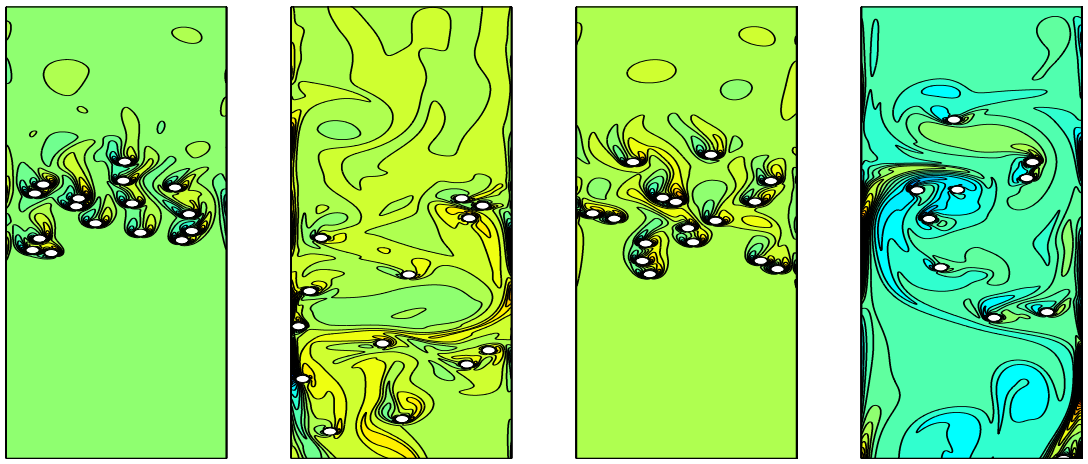

(a) Without heat & mass transfer (b) With heat transfer (c) With mass transfer (d) With heat & mass transfer

Figure 8: Vortex distribution around the particles at $t/(D_p^2/\nu)=2$.

settling velocity of the particles increasing, the particle-particle interaction is enforced, which leads to the more intense oscillation of $\overline{v}$ of the cases with heat transfer.

Next, to describe the variance of the motion of the particle cluster, the velocity fluctuation of the particle cluster is calculated,

$$\tilde{\boldsymbol{u}}=(\tilde{u},\tilde{v})=\frac{\sqrt{\sum_i(\boldsymbol{u}_i-\overline{\boldsymbol{u}_c})^2}}{N}. \tag{5.2}$$

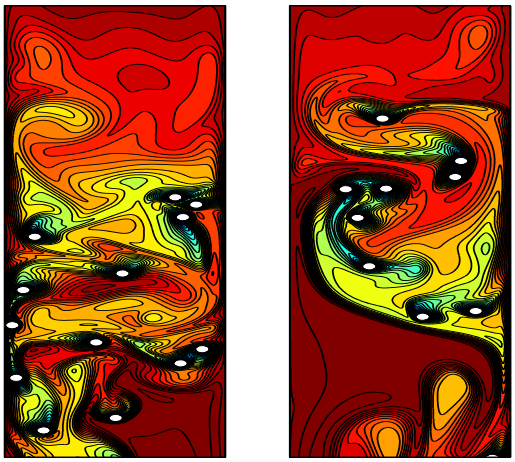

(a) With heat transfer (b) With heat & mass transfer

Figure 9: Temperature distribution around the particles at $t/(D_p^2/\nu)=2$.

Fig. 10 shows the time history of the velocity fluctuation of the particle cluster in the horizontal and vertical directions. It is observed that both $\tilde{u}$ and $\tilde{v}$ experience two phases, namely, monotonic increase and oscillation. At the beginning, the particles distribute closely, the strong particle-particle interaction is apt to disperse the particles, consequently, $\tilde{u}$ and $\tilde{v}$ increase monotonically. With the particles colliding with each other, the particles move disorderly, which leads to the oscillation of $\tilde{u}$ and $\tilde{v}$. Furthermore, compared to the cases without heat transfer, $\tilde{u}$ and $\tilde{v}$ of the cases with heat transfer are much larger, namely, the motion of the particles is more inhomogeneous. The downward thermal convection pushes the particles to move downward, the average settling velocity of the particles is larger, and the particles collide with each other more frequently, consequently, $\tilde{u}$ and $\tilde{v}$ of the cases with heat transfer are much larger.

Since the particles are composed of two components, one insoluble while the other soluble, with mass transfer, the mass and moment inertia of the particles decrease, and the result is that the motion of the particles is more sensitive to the fluid flow. Fig. 11 shows the concentration distribution around the particles at $t/(D_p^2/\nu)=2$. Without heat transfer, the concentration distribution around the particles is obvious, while the rate of mass transfer is approaching zero under the effect of thermal convection, namely, the rate of mass transfer of the case with heat transfer is higher than that of the case without heat transfer. The average settling velocity of the particles of the case with heat transfer is larger, where the convection mass transfer is enforced, consequently, the rate of mass transfer of the case with heat transfer is higher.

Besides the average settling velocity and the velocity fluctuation, to represent the inhomogeneity of the distribution of the particles, the ensemble dispersion of the particle

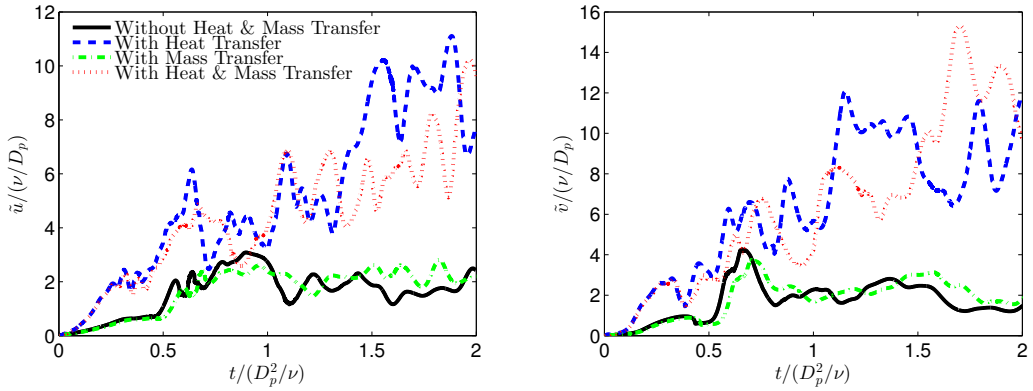

(a) Horizontal direction (b) Vertical direction

Figure 10: Time history of the velocity fluctuation of the particle cluster in the horizontal (a) and vertical (b) directions.

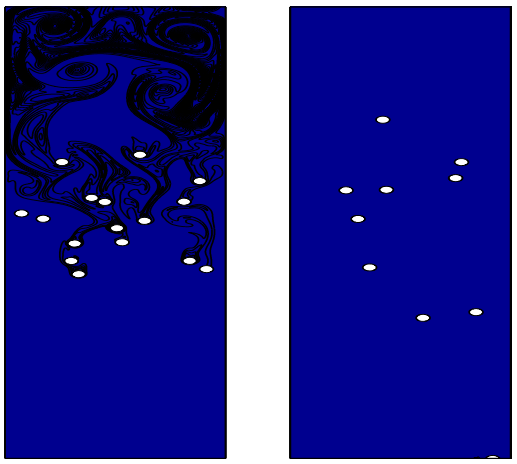

(a) With mass transfer (b) With heat & mass transfer

Figure 11: Concentration distribution around the particles at $t/(D_p^2/\nu)=2$.

cluster is calculated,

$$\boldsymbol{D}=(D_x,D_y)=\frac{\sqrt{\sum_i(\boldsymbol{x}_i-\overline{\boldsymbol{x}_c})^2}}{N}, \tag{5.3}$$

where $\overline{\boldsymbol{x}_c}=\sum_i \boldsymbol{x}_i/N$ is the average position of the particle cluster. It is clear that the smaller the ensemble dispersion is, the more homogeneous the distribution of the particle cluster is, while the distribution of the particle cluster is more inhomogeneous with the ensemble dispersion increasing. Fig. 12 shows the time history of the ensemble dispersion of

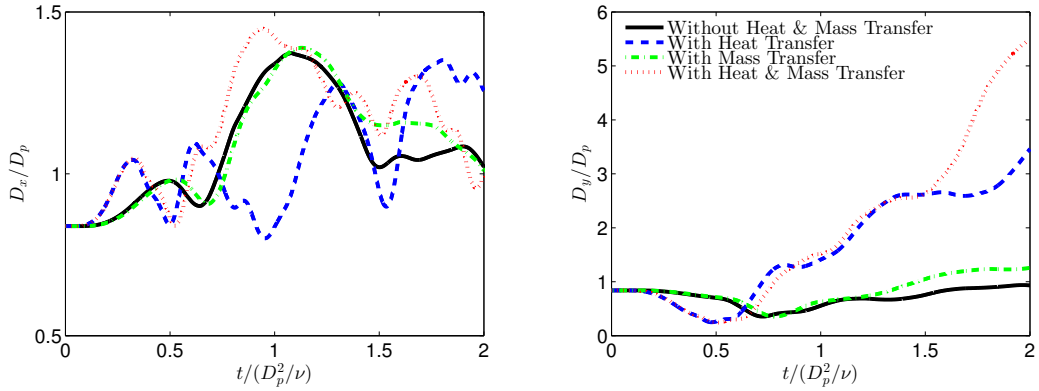

(a) Horizontal direction (b) Vertical direction

Figure 12: Time history of the ensemble dispersion of the particle cluster in the horizontal (a) and vertical (b) directions.

the particle cluster in the horizontal and vertical directions. In the horizontal direction, after a transient monotonic increase at the beginning, D_x oscillates. At the beginning, the particles distribute closely, the strong particle-particle interaction is apt to disperse the particles, and the result is that the distribution of the particles is more inhomogeneous. With the particles approaching the channel walls, D_x reaches its maximum, and the wall confinement suppresses the dispersion of the particles, pushing the particles toward the channel centerline. Finally, the dispersion of the particles and the confinement of the channel walls compete with each other, the distribution of the particles reaches a dynamic equilibrium, and D_x oscillates. Compared to the cases without heat transfer, D_x of the cases with heat transfer increases more rapidly at the beginning. Firstly, thermal convection makes the particle-particle interaction become stronger, and the particles become more disperse. Besides, the mass of the particles decreases due to mass transfer, and the motion of the particles is more easily affected by the fluid flow, the distribution of the particles is more inhomogeneous, namely, D_x increases more rapidly. In the vertical direction, after a transient decrease, D_y increases monotonically. Compared to the cases without heat transfer, D_y of the cases with heat transfer increases more rapidly. The particles are cold while the fluid is hot, the downward thermal convection pushes the particles to move downward. Since the average settling velocity of the particles of the cases with heat transfer is larger than that of the cases without heat transfer, the particle-particle interaction becomes stronger, and the particles collide with each other more frequently, which is conducive to the dispersion of the particles, compared to the cases without heat transfer, the inhomogeneity of the distribution of the particle cluster increases.

6 Conclusions

The sedimentation of a particle cluster with heat and mass transfer is studied with the lattice Boltzmann method, where the effect of thermal convection and mass transfer on the motion of the particle cluster is investigated. Compared to the cases without heat transfer, the motion of the particle cluster of the cases with heat transfer is quite different, including the average settling velocity, velocity fluctuation and ensemble dispersion. Specifically, the following conclusions are drawn:

- compared to mass transfer, the effect of thermal convection is more dominant, which affects the motion of the particle cluster significantly;
- the average settling velocity of the particle cluster oscillates around zero, which is the competitive result between the particle dispersion and the wall confinement;
- the particle-particle interaction is enforced by thermal convection, and the velocity fluctuation of the particle cluster is much more intense;
- with mass transfer, the mass and moment inertia of the particle decrease, and the motion of the particle cluster is more sensitive to the fluid flow, the distribution of the particle cluster is more inhomogeneous.

Since the motion of the particle cluster with heat and mass transfer is complex, the present study is limited. For example, the conjugate heat transfer between the particles and the fluid, the density and initial volume fraction of the soluble component, are not considered. To deepen our understanding of the non-isothermal and volatile particulate flows, numerous detailed works should be conducted in the future.

Acknowledgements

The project is supported by the China Postdoctoral Science Foundation (2022M720027).

References

[1] Z. Feng and E. Michaelides, *The immersed boundary-lattice Boltzmann method for solving fluid-particles interactions problems,* J. Comput. Phys., 195 (2004), pp. 602–628.
[2] A. Zaidi, T. Tsuji and T. Tanaka, *Hindered settling velocity & structure formation during particle settling by direct numerical simulation,* Procedia Eng., 102 (2015), pp. 1656–1666.
[3] X. Zhang, H. Liu and Y. Zhang, *Direct numerical simulation of the sedimentation of a particle pair in a shear-thinning fluid,* Phys. Rev. Fluids, 5 (2020), 014304.
[4] M. Li, H. Liu and Y. Zhang, *Two-dimensional characterization of particle entrainment over a downstream obstacle,* Int. J. Multiphase Flow, 156 (2022), 104228.
[5] H. Gan, J. Chang, J. Feng and H. Hu, *Direct numerical simulation of the sedimentation of solid particles with thermal convection,* J. Fluid Mech., 481 (2003), pp. 385–411.

[6] Z. YU, X. SHAO AND A. WACHS, *A fictitious domain method for particulate flows with heat transfer,* J. Comput. Phys., 217 (2006), pp. 424–452.
[7] F. MANDUJANO AND R. RECHTMAN, *Thermal levitation,* J. Fluid Mech., 606 (2008), pp. 105–114.
[8] Z. FENG AND E. MICHAELIDES, *Heat transfer in particulate flows with Direct Numerical Simulation (DNS),* Int. J. Heat Mass Transf., 52 (2009), pp. 777–786.
[9] S. WANG, G. LIU AND Y. WU, *Numerical investigation of gas-to-particle cluster convective heat transfer in circulating fluidized beds,* Int. J. Heat Mass Transf., 53 (2010), pp. 3102–3110.
[10] S. KANG AND Y. HASSAN, *A direct-forcing immersed boundary method for the thermal lattice Boltzmann method,* Comput. Fluids, 49 (2011), pp. 36–45.
[11] D. KIM, H. YOON AND M. HA, *Particle behavior in a vertical channel with thermal convection in the low Grashof number regime,* Comput. Fluids, 48 (2011), pp. 183–191.
[12] Z. FENG AND S. MUSONG, *Direct numerical simulation of heat and mass transfer of spheres in a fluidized bed,* Powder Tech., 262 (2014), pp. 62–70.
[13] A. ESHGHINEJADFARD AND D. THEVENIN, *Numerical simulation of heat transfer in particulate flows using a thermal immersed boundary lattice Boltzmann method,* Int. J. Heat Fluid Flow, 60 (2016), pp. 31–46.
[14] B. YANG, S. CHEN, C. CAO, Z. LIU AND C. ZHENG, *Lattice Boltzmann simulation of two cold particles settling in Newtonian fluid with thermal convection,* Int. J. Heat Mass Transf., 93 (2016), pp. 477–490.
[15] G. BATCHELOR, *Mass transfer from a particle suspended in fluid with a steady linear ambient velocity distribution,* J. Fluid Mech., 95 (1979), pp. 369–400.
[16] Z. FENG AND E. MICHAELIDES, *Unsteady heat and mass transfer from a spheroid,* AIChE J., 43 (1997), pp. 609–614.
[17] G. SUBRAMANIAN AND D. KOCH, *Inertial effects on the transfer of heat or mass from neutrally buoyant spheres in a steady linear velocity field,* Phys. Fluids, 18 (2006), 073302.
[18] S. WANG, Y. XU AND H. LU, *CFD studies on mass transfer of gas-to-particle cluster in a circulating fluidized bed,* Comput. Chem. Eng., 33 (2009), pp. 393–401.
[19] C. YANG, J. ZHANG, D. KOCH DAND X. YIN, *Mass/heat transfer from a neutrally buoyant sphere in simple shear flow at finite Reynolds and Peclet numbers,* AIChE J., 57 (2011), pp. 1419–1433.
[20] W. JODREY AND E. TORY, *Computer simulation of isotropic, homogeneous, dense random packing of equal spheres,* Powder Tech., 30 (1981), pp. 111–118.
[21] N. KARAYIANNIS AND M. LASO, *Monte Carlo scheme for generation and relaxation of dense and nearly jammed random structures of freely jointed hard-sphere chains,* Macromolecules, 41 (2008), pp. 1537–1551.
[22] Y. QIAN AND P. LALLEMAND, Lattice BGK Models for Navier-Stokes Equation, IOP Publishing, 17 (1992), pp. 479–484.
[23] Z. GUO, C. ZHENG AND B. SHI, *Discrete lattice effects on the forcing term in the lattice Boltzmann method,* Phys. Rev. E, 65 (2002), 046308.
[24] Z. CHAI AND B. SHI, *Multiple-relaxation-time lattice Boltzmann method for the Navier-Stokes and nonlinear convection-diffusion equations: Modeling, analysis, and elements,* Phys. Rev. E, 102 (2020), 023306.
[25] C. PENG, Y. TENG, B. HWANG, Z. GUO AND L. WANG, *Implementation issues and benchmarking of lattice Boltzmann method for moving rigid particle simulations in a viscous flow,* Comput. Math. Appl., 72 (2016), pp. 349–374.
[26] S. TAO, J. HU AND Z. GUO, *An investigation on momentum exchange methods and refilling*

algorithms for lattice Boltzmann simulation of particulate flows, Comput. Fluids, 133 (2016), pp. 1–14.

[27] D. NOBLE AND J. TORCZYNSKI, *A lattice-Boltzmann method for partially saturated computational cells,* Int. J. Modern Phys. C, 09 (1998), pp. 1189–1201.

[28] J. LIU, C. HUANG AND Z. CHAI, *A diffuse-interface lattice Boltzmann method for fluid–particle interaction problems,* Comput. Fluids, 233 (2022), 105240.

[29] J. HU, S. TAO AND Z. GUO, *An efficient unified iterative scheme for moving boundaries in lattice Boltzmann method,* Comput. Fluids, 144 (2017), pp. 34–43.

[30] J. HU, M. XU AND J. ZHANG, *A consistent treatment of moving boundaries with thermal convection for lattice Boltzmann method,* Phys. Fluids, 33 (2021), 123312.

[31] B. WEN, C. ZHANG, Y. TU, C. WANG AND H. FANG, *Galilean invariant fluid–solid interfacial dynamics in lattice Boltzmann simulations,* J. Comput. Phys., 266 (2014), pp. 161–170.

[32] D. WAN AND S. TUREK, *Direct numerical simulation of particulate flow via multigrid FEM techniques and the fictitious boundary method,* Int. J. Numer. Methods Fluids, 51 (2006), pp. 531–566.

[33] Q. CHEN, X. ZHANG AND J. ZHANG, *Improved treatments for general boundary conditions in the lattice Boltzmann method for convection-diffusion and heat transfer processes,* Phys. Rev. E, 88 (2013), 033304.